Spin-orbit torque for field-free switching in C_{3v} crystals

Diego García Ovalle,* Armando Pezo,† and Aurélien Manchon‡
Aix-Marseille Université, CNRS, CINaM, Marseille, France

(Received 22 December 2022; accepted 6 March 2023; published 20 March 2023)

Spin-orbit torques in noncentrosymmetric polycrystalline magnetic heterostructures are usually described in terms of field-like and damping-like torques. However, materials with a lower symmetry point group can exhibit torques whose behavior substantially deviates from the conventional ones. In particular, based on symmetry arguments it was recently proposed that systems belonging to the C_{3v} point group display spin-orbit torques that can promote field-free switching [Liu *et al.*, Nat. Nanotechnol. **16**, 277 (2021)]. In the present work, we analyze the general form of the torques expected in C_{3v} crystals using the invariant theory. We uncover several new components that arise from the coexistence of the threefold rotation and mirror symmetries. Using both tight binding model and first principles simulations, we show that these unconventional torque components arise from the onset of trigonal warping of the Fermi surface and can be as large as the damping-like torque. In other words, the Fermi surface warping is a key indicator to the onset of field-free switching in low symmetry crystals.

DOI: 10.1103/PhysRevB.107.094422

I. INTRODUCTION

Electrical manipulation of the magnetization in single magnetic thin films using spin-orbit torques has become routinely available in the past decade [1]. In perpendicularly magnetized systems, the most suitable configuration for memory applications, achieving reversible current-driven switching necessitates the combination of spin-orbit torque with an external magnetic field [2,3]. As a matter of fact, whereas the spin-orbit torque tends to bring the magnetization in the plane, applying an additional external field along the current direction provides the necessary force that completes the reversal process in a deterministic manner. The need for this external field is considered as a hurdle for memory applications and several strategies have been proposed to circumvent this difficulty. Field-free current-driven switching has been realized using exchange bias from a neighboring antiferromagnet [4,5], exchange coupling [6,7], or anomalous Hall torque from a proximate ferromagnet [8,9]. The latter takes advantage of an interfacial spin rotation of the incoming spin current [10], sometimes called spin swapping [11,12] (see also Refs. [13,14]). In addition, structural engineering has been successfully exploited to design lateral [15–19] and geometrical [20] symmetry breaking, tilted anisotropy [21–23], and longitudinal (compositional or structural) gradient [24,25].

Whereas most of these works considered multilayers made out of polycrystalline materials, recent experiments have demonstrated that low symmetry crystals are endowed with unconventional spin-orbit torques that can play the role of an external field, thereby completing the current-driven switching process. The impact of the crystalline symmetries on the spin-orbit torque is well known since its initial observation in the noncentrosymmetric magnetic semiconductors (Ga,Mn)As [26,27] and in the Heusler alloy MnNiSb [28], where the bulk inversion symmetry breaking promotes a so-called Dresselhaus-like spin-orbit torque. In fact, further lowering of the crystalline symmetries can lead to unusual torques that turn out to be instrumental to achieve field-free switching. For instance, WTe_2 has been shown to display a "perpendicular damping-like torque" [29,30] that enables field-free switching, an effect confirmed in several experiments [31–33]. This torque, also present in $MoTe_2$ [34] and $NbSe_2$ [35], is associated with a crystalline mirror symmetry breaking perpendicular to the interface plane. When a current is injected along this mirror, it may generate a nonequilibrium spin density contained in this mirror plane and normal to the interface. Antiferromagnets are also currently attracting attention from this standpoint. Indeed, the combination of crystalline and magnetic symmetries tend to produce spin currents with a polarization different from what is dictated by the conventional spin Hall effect [36,37], an effect sometimes called "magnetic" spin Hall effect [38,39]. These spin currents can in turn exert "unconventional" torques on an adjacent ferromagnet, as observed in collinear (Mn_2Au [40] and RuO_2[41,42]) and noncollinear antiferromagnets (Mn_3GaN [43], Mn_3Pt [44], and Mn_3Sn [45]).

Recently, Liu *et al.* [46] studied the current-driven magnetization reversal in a crystalline CuPt/CoPt bilayer in the $L1_1$ phase grown along the (111) direction. They reported that field-free switching could be achieved when the current was applied along low-symmetry crystallographic directions. Intriguingly, the polarity of the magnetization reversal loop displayed a periodic pattern depending on the crystallographic direction along which the current was applied. This unusual behavior was interpreted as arising from an unconventional torque, tagged "3m" torque, which appears in crystals with the C_{3v} point group [47]. Nonetheless, no microscopic explanation was proposed to explain the emergence of the 3m torque in this bilayer. Such an explanation is highly desired,

*diego-fernando.garcia-ovalle@univ-amu.fr
†armando-arquimedes.pezo-lopez@univ-amu.fr
‡aurelien.manchon@univ-amu.fr

TABLE I. Character table of the C_{3v} point group. (x, y, z) are the components of a polar vector, whereas (m_x, m_y, m_z) are the components of an axial vector.

	E	$2C_3$	$3\sigma_v$	Linear	Quadratic	Cubic
A_1	1	1	1	z	x^2+y^2, z^2 $m_x^2+m_y^2, m_z^2$	$z^3, z(x^2+y^2), x(x^2-3y^2)$ $m_y(3m_x^2-m_y^2)$
A_2	1	1	-1	m_z		$y(3x^2-y^2)$ $m_x(m_x^2-3m_y^2)$
E	2	-1	0	(x, y) (m_x, m_y)	$(x^2-y^2, xy), (xz, yz)$ $(m_x^2-m_y^2, m_xm_y)$ (m_xm_z, m_ym_z)	$[z(x^2-y^2), xyz], (xz^2, yz^2), [x(x^2+y^2), y(x^2+y^2)]$ $[m_z(m_x^2-m_y^2), m_xm_ym_z], (m_xm_z^2, m_ym_z^2)$ $[m_x(m_x^2+m_y^2), m_y(m_x^2+m_y^2)]$

especially with the acceleration of the research in two-dimensional van der Waals magnets [48]. As a matter of fact, most of the van der Waals magnets possess a hexagonal or trigonal point group and are therefore entitled to display such a torque. For instance, the 3m torque was identified in Fe_3GeTe_2 monolayer [49,50] and is associated with an unconventional form of Dzyaloshinskii-Moriya interaction [51]. Nonetheless, mere symmetry consideration is not sufficient and a microscopic description is needed. Indeed, recent first principles calculation in the Janus monolayer VSeTe demonstrated that, although this material possesses the C_{3v} symmetry, no "unconventional" torque can be obtained and only the usual field-like and damping-like torques are present [52]. Therefore, understanding the physical origin of the 3m torque in C_{3v} crystals and suggesting guidelines to enhance it is of crucial interest.

In this work, we intend to clarify the nature of the spin-orbit torque in crystals with C_{3v} point group, i.e., its vectorial form and its microscopic origin. We first determine the general form of the spin-orbit torque up to the third order in magnetization using the invariant theory applied on the C_{3v} character table. We then consider a minimal model for a magnetic gas with C_{3v} symmetries. In this model, the spin texture is governed by the cooperation between linear (Rashba) and cubic spin-momentum locking terms. The Fermi surface is characterized by trigonal warping that appears close to the top of the band structure. We show that the unconventional 3m torque is associated with the cubic spin-momentum locking when the Fermi surface displays strong trigonal warping. We therefore suggest that trigonal warping can be used as a good indicator for the search of 3m torques in C_{3v} crystals and two-dimensional van der Waals magnets.

II. SYMMETRY ANALYSIS

We first determine the general form of the torque using the representation theory [53,54]. The C_{3v} point group is characterized by the identity E, the threefold rotation along $\mathbf{z}$, C_3, and the mirror symmetry normal to, say, $\mathbf{y}$, σ_v. It has three irreducible representations A_1, A_2, and E, i.e., matrices *representing* the action of the symmetry operations E, C_3, and σ_v. Although a given symmetry operation can be represented by an infinite number of matrices, the trace of these representative matrices is unique for a given operation. Therefore, each irreducible representation can be identified by a unique set of traces called "characters." Table I gives the character table of the C_{3v} point group. The (equilibrium and nonequilibrium) properties of a given crystal are written as the combination of polar and axial vectors. For instance, in the case of the spin-orbit torque these vectors are the electric field (E_x, E_y, E_z) (polar vector) and the magnetization (m_x, m_y, m_z) (axial vector). Concretely, they transform in the following way:

$$(E_x, E_y) \xrightarrow{\sigma_v} (E_x, -E_y), \tag{1}$$

$$(E_x, E_y) \xrightarrow{C_3} \left(-\frac{1}{2}E_x - \frac{\sqrt{3}}{2}E_y, \frac{\sqrt{3}}{2}E_x - \frac{1}{2}E_y\right) \tag{2}$$

and

$$(m_x, m_y, m_z) \xrightarrow{\sigma_v} (-m_x, m_y, -m_z), \tag{3}$$

$$(m_x, m_y, m_z) \xrightarrow{C_3} \left(-\frac{1}{2}m_x - \frac{\sqrt{3}}{2}m_y, \frac{\sqrt{3}}{2}m_x - \frac{1}{2}m_y, m_z\right). \tag{4}$$

When applying the symmetry operations on these vectors' components, they transform according to the irreducible representations A_1, A_2, and E so that one can define *basis functions* for each representation. In Table I, we give the basis functions of the irreducible representation of the C_{3v} point group up to the third order in magnetization.

Let us determine the general form of the torque based on Table I. The spin-orbit torque $\boldsymbol{\tau}$ is associated with an effective field, $\boldsymbol{\tau} = -\gamma\mathbf{m}\times\mathbf{h}$. This effective field $\mathbf{h}$ is an axial vector, like $\mathbf{m}$, so its component h_z and (h_x, h_y) belong to A_2 and E, respectively, and can be expanded as combinations of the invariant basis functions given in Table I. The only possible combinations of magnetization components with $\mathbf{E}$ that are invariant under the symmetries of the group are m_z, m_z^3, and $m_x(m_x^2-3m_y^2)$, that all belong to A_2. Conversely, $\mathbf{z}\times\mathbf{E}$ is an axial vector and hence its allowed combinations are 1, m_z, and $m_y(3m_x^2-m_y^2)$, that all belong to A_1. Accounting for all combinations involving polar vector components at the first order and axial vector components up to the third order in magnetization, we obtain

$$\begin{aligned}\boldsymbol{h}_\parallel = {} & h_{\mathrm{FL}}^{\parallel}\left[1+\eta_{\mathrm{FL}}m_z^2+\delta_{\mathrm{FL}}m_y\left(3m_x^2-m_y^2\right)\right]\mathbf{z}\times\mathbf{E} \\ & + h_{\mathrm{DL}}^{\parallel}\left[\left(1+\eta_{\mathrm{DL}}m_z^2\right)m_z+\delta_{\mathrm{DL}}m_x\left(m_x^2-3m_y^2\right)\right]\mathbf{E} \\ & + \left[h_{3\mathrm{m}}^{\parallel}m_x\left(1+\eta_{3\mathrm{m}}m_z^2\right)+h_{3\mathrm{m}}^{z}m_zm_y-2h_{\mathrm{PH}}^{\parallel}m_xm_y\right. \\ & \left. + h_{\chi}^{\parallel}m_z\left(m_x^2-m_y^2\right)\right](E_x\mathbf{x}-E_y\mathbf{y})\end{aligned}$$

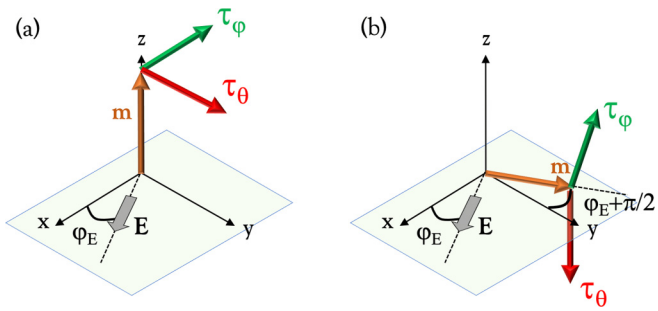

FIG. 1. Schematics of the torque components when the magnetization is (a) perpendicular to the plane and (b) in the plane, at 90° of the applied electric field.

$$+\big[-h_{3\mathrm{m}}^{\parallel}m_y\big(1+\eta_{3\mathrm{m}}m_z^2\big)+h_{3\mathrm{m}}^{z}m_zm_x+h_{\mathrm{PH}}^{\parallel}\big(m_x^2-m_y^2\big)+2h_{\chi}^{\parallel}m_xm_ym_z\big](E_y\mathbf{x}+E_x\mathbf{y}), \tag{5}$$

$$\boldsymbol{h}_{\perp}=\big\{h_{\mathrm{DL}}^{z}\big(1+\eta_z m_z^2\big)\mathbf{E}\cdot\mathbf{m}+h_{\mathrm{FL}}^{z}m_z\mathbf{m}\cdot(\mathbf{z}\times\mathbf{E})+h_{\mathrm{PH}}^{z}\big[\big(m_x^2-m_y^2\big)E_y+2m_xm_yE_x\big]+h_{\chi}^{z}m_z\big[\big(m_x^2-m_y^2\big)E_x-2m_xm_yE_y\big]\big\}\mathbf{z}. \tag{6}$$

The formulas given above are general and they do not rely on any specific microscopic mechanism. We recognize the field-like torque ($h_{\mathrm{FL}}^{\parallel,z}$), the damping-like torque ($h_{\mathrm{DL}}^{\parallel,z}$), and the 3m torque reported in Refs. [46,49] ($h_{3\mathrm{m}}^{\parallel,z}$). At higher orders, these terms are modulated by a planar anisotropy term, $\sim\eta_\alpha$, and a trigonal anisotropy term, $\sim\delta_\alpha$. In addition, the magnitude of the field-like and damping-like torques are different in plane ($h_{\mathrm{FL}}^{\parallel}$, $h_{\mathrm{DL}}^{\parallel}$) and out of plane ($h_{\mathrm{FL}}^{z}$, h_{DL}^{z}). By removing these anisotropies, i.e., by setting $\eta_{\mathrm{FL,DL}}=0$, $\delta_{\mathrm{FL,DL}}=0$, and $h_{\mathrm{FL,DL}}^{\parallel}=h_{\mathrm{FL,DL}}^{z}$, one retrieves the effective fields associated with the conventional field-like and damping-like torques, i.e., $\sim\mathbf{z}\times\mathbf{E}$ and $\sim(\mathbf{z}\times\mathbf{E})\times\mathbf{m}$.

In addition, we also identify two additional torques that we refer to as in-plane ($h_{\mathrm{PH}}^{\parallel}$) and out-of-plane ($h_{\mathrm{PH}}^{z}$) planar Hall torque and chiral torques ($h_{\chi}^{\parallel,z}$). The planar Hall torque possesses symmetries comparable to the planar Hall effect: it is active when the magnetization lies in the $(\mathbf{x},\mathbf{y})$ plane and its magnitude depends on the angle between the electric field and the magnetization. The chiral torque necessitates canting the magnetization away from the plane and it changes sign when reversing the magnetization ($m_z\to -m_z$).

To clarify the impact of the torque on the magnetization dynamics, we analyze its expression in two illustrative situations. When the magnetization lies out of plane ($\mathbf{m}=\mathbf{z}$), which is typical of perpendicularly magnetized systems at rest [see Fig. 1(a)], the two torque components up to first order in magnetization read

$$\boldsymbol{\tau}_{\parallel}=-\gamma h_{\mathrm{FL}}^{\parallel}\mathbf{z}\times(\mathbf{z}\times\mathbf{E}), \tag{7}$$

$$\boldsymbol{\tau}_{\perp}=-\gamma h_{\mathrm{DL}}^{\parallel}\mathbf{z}\times\mathbf{E}. \tag{8}$$

We see that only the conventional field-like and damping-like torques are active in this configuration. One can see that the field-like torque is always along the electric field, $\sim\mathbf{m}\times(\mathbf{z}\times\mathbf{E})$, whereas the damping-like torque is perpendicular to it, $\sim\mathbf{m}\times[(\mathbf{z}\times\mathbf{E})\times\mathbf{m}]$. These two torques are the ones that destabilize the magnetization from its rest position and tend to bring it in the plane, normal to the applied electric field [see Fig. 1(b)].

Once the magnetization is in plane, at $\phi=\varphi_E+\frac{\pi}{2}$, where φ_E is the in-plane angle of the electric field with respect to $\mathbf{x}$ and (θ,ϕ) are the polar and azimuthal angles of the magnetization unit vector, the torques $\boldsymbol{\tau}=-\gamma\mathbf{m}\times\mathbf{h}=\tau_\theta\mathbf{e}_\theta+\tau_\phi\mathbf{e}_\phi$ in regular spherical coordinates are

$$\tau_\theta/E=\gamma[h_{\mathrm{DL}}\delta_{\mathrm{DL}}-h_{3m}]\sin 3\varphi_E, \tag{9}$$

$$\tau_\phi/E=\gamma h_{\mathrm{PH}}^{z}\cos 3\varphi_E. \tag{10}$$

In this configuration, the conventional field-like and damping-like torques are quenched and the only active torques are the 3m torque ($h_{3\mathrm{m}}^{\parallel}$), identified in Ref. [46], the trigonal anisotropy correction to the damping-like torque ($h_{\mathrm{DL}}^{\parallel}\delta_{\mathrm{DL}}$), and the perpendicular planar Hall torque (h_{PH}^{z}). Here, only τ_θ induces the deterministic switching, which means that the 3m torque and the trigonal anisotropy correction to the damping-like torque are the active contributions in this process. Remarkably, in this frame the two other torques identified in Eqs. (5) and (6), i.e., the planar Hall torque ($h_{\mathrm{PH}}^{\parallel,z}$) and the chiral torque ($h_{\chi}^{\parallel,z}$), are only active when $\theta\neq 0,\pi/2$ and should therefore impact the magnetization dynamics itself. Their influence could modify the current-driven auto-oscillation [55,56], a phenomenon that we leave to future studies.

III. PHYSICAL ORIGIN OF THE UNCONVENTIONAL TORQUES

A. Minimal tight-binding model for C_{3v} magnets

The symmetry analysis provided above does not give information about the relative magnitude of the different torques. To better understand which microscopic mechanisms control these different components, we now turn our attention towards a minimal model for the spin-orbit torque. We consider a ferromagnetic system defined in a hexagonal lattice as depicted on Fig. 2(a) with C_{3v} symmetry modeled by the Hamiltonian

$$\mathcal{H}_0=\varepsilon_{\mathbf{k}}+\Delta\boldsymbol{\sigma}\cdot\mathbf{m}+\mathcal{H}_{\mathrm{R}}+\mathcal{H}_{\mathrm{R3}}, \tag{11}$$

with

$$\mathcal{H}_{\mathrm{R}}=-i\frac{t_{\mathrm{R}}}{a}\sum_{\mathbf{u},s=\pm}s\boldsymbol{\sigma}\cdot(\mathbf{z}\times\mathbf{u})e^{is\mathbf{k}\cdot\mathbf{u}}=\frac{t_{\mathrm{R}}}{a}\boldsymbol{\eta}_{\mathbf{k}}\cdot(\boldsymbol{\sigma}\times\mathbf{z}), \tag{12}$$

$$\mathcal{H}_{\mathrm{R3}}=-it_{\mathrm{R3}}\sum_{\mathbf{u},s=\pm}s\boldsymbol{\sigma}\cdot\mathbf{z}e^{is\mathbf{k}\cdot\mathbf{u}}=t_{\mathrm{R3}}\boldsymbol{\lambda}_{\mathbf{k}}\sigma_z. \tag{13}$$

The sum is taken over the nearest neighbors, i.e., $\mathbf{u}=\mathbf{a},\mathbf{b},\mathbf{c}$, sketched on Fig. 2(a), and a is the lattice parameter. Explicitly, $\varepsilon_{\mathbf{k}}=-2t(\cos\mathbf{k}\cdot\mathbf{a}+\cos\mathbf{k}\cdot\mathbf{b}+\cos\mathbf{k}\cdot\mathbf{c})$, $\boldsymbol{\eta}_{\mathbf{k}}=2(\mathbf{a}\sin\mathbf{k}\cdot\mathbf{a}+\mathbf{b}\sin\mathbf{k}\cdot\mathbf{b}+\mathbf{c}\sin\mathbf{k}\cdot\mathbf{c})$, and $\boldsymbol{\lambda}_{\mathbf{k}}=2(\sin\mathbf{k}\cdot\mathbf{a}+\sin\mathbf{k}\cdot\mathbf{b}+\sin\mathbf{k}\cdot\mathbf{c})$. Here, t is the nearest-neighbor hopping parameter, Δ is the exchange between the conduction electrons and the magnetization $\mathbf{m}$, t_R is the linear Rashba spin-orbit coupling coming from inversion symmetry

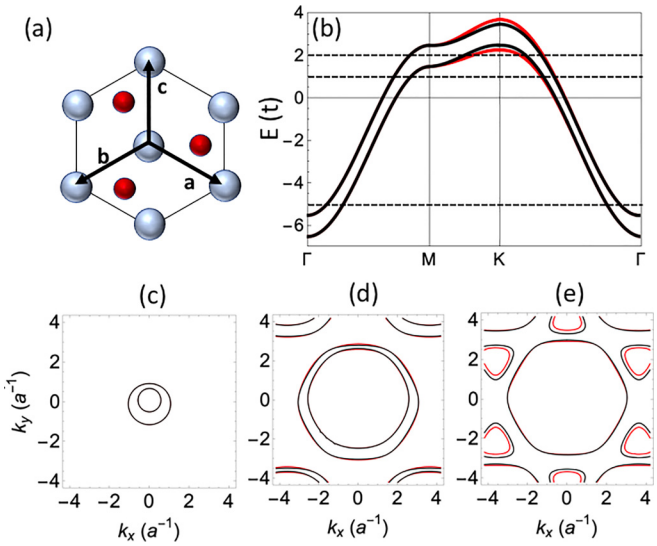

FIG. 2. (a) Unit cell of the minimal model for the C_{3v} crystal. The gray atoms represent the hexagonal lattice sites and the red atoms break the plane inversion symmetry while conserving the threefold rotation along **z** and the mirror symmetry normal to **y**. (b) Band structure of the tight-binding model described in the text with $t_R = 0.1t$ and $\Delta = 0.5t$, for the cases $t_{R3} = 0$ (black lines) and $t_{R3} = 0.1t$ (red lines). The magnetization direction is set to $\theta = \frac{\pi}{2}$ and $\phi = 0$. The horizontal dashed lines correspond to $\mu = -5t$, $\mu = t$, and $\mu = 2t$, respectively. (c)–(e) Fermi surfaces with ($t_{R3} = 0.1t$, red lines) and without ($t_{R3} = 0$, black lines) cubic spin-orbit coupling for (c) $\mu = -5t$, (d) $\mu = t$, and (e) $\mu = 2t$.

breaking normal to the (**a**, **b**) plane, and t_{R3} is its cubic correction that is associated with the mirror symmetry normal to the **y** axis.

This model enhances the conventional free-electron Rashba gas by adding two ingredients: (i) the hexagonal symmetry and (ii) the cubic spin-orbit coupling. Figure 2(b) represents the band structure for a standard set of parameters with (red lines) and without (black lines) cubic spin-orbit coupling. One directly sees that the cubic spin-orbit coupling only modifies the band structure close to the top of the band. The Fermi surface at three characteristic fillings are sketched on Figs. 2(c)–2(e), with (red lines) and without (black lines) cubic spin-orbit coupling. At low band filling [Fig. 2(c)], where the dispersion is mostly quadratic, the Fermi surface is spherical and the cubic spin-orbit coupling has almost no impact. We therefore expect that the torque reduces to its most conventional form, field-like and damping-like. Upon increasing the band filling [Figs. 2(d) and 2(e)], the Fermi surface starts displaying hexagonal warping and the cubic spin-orbit coupling modifies the energy contours. In this context, at high band filling the warping is strong with Fermi pockets appearing away from the Γ point. Turning on the cubic spin-orbit coupling modifies the Fermi surface, resulting in a strong trigonal warping. It is clear that the unconventional torques identified in the previous section are expected to emerge in this regime.

The impact of Fermi surface warping on the spin-orbit torque has been addressed theoretically in the context of the topological insulator surfaces. Kurebayashi and Nagaosa [57] and Imai *et al.* [58] investigated the influence of warping on the spin-transfer torque and spin-orbit torque, respectively, in magnetic domain walls and skyrmions to the first order of the magnetization gradient. The spin-orbit torque discussed presently is not addressed in these works. Zhou *et al.* [59] investigated the appearance of a damping-like torque that is nonlinear in electric field and directly induced by the warping. Li *et al.* [60] investigated the impact of the hexagonal warping on the spin-orbit torque, linear in electric field, and observed that the torque does not vanish when the magnetization lies in the plane. This is consistent with the analysis performed in the previous section, although a direct connection with the general form provided in Eqs. (5) and (6) remains difficult.

Let us now compute the effective spin-orbit field driven by the current, $\mathbf{h} = (\Delta/VM_s)\langle\boldsymbol{\sigma}\rangle$, where M_s is the saturation magnetization of the ferromagnet, V is the volume of the unit cell, and $\langle\ldots\rangle$ denotes nonequilibrium quantum statistical averaging. $\langle\boldsymbol{\sigma}\rangle$ is computed within the linear response formalism considering the symmetrized decomposition of the Kubo-Bastin formula proposed in Ref. [61], which takes the form

$$\langle\hat{\sigma}_i\rangle_{\rm Int} = -\frac{e\hbar}{4\pi}\int f(\epsilon)d\epsilon\ {\rm Re}[{\rm Tr}\{\hat{\mathbf{v}}(G^{\rm R-A})\hat{\sigma}_i(\partial_\epsilon G^{\rm R+A})\}], \tag{14}$$

$$\langle\hat{\sigma}_i\rangle_{\rm Ext} = -\frac{e\hbar}{8\pi}\int \partial_\epsilon f(\epsilon)d\epsilon\ {\rm Re}[{\rm Tr}\{\hat{\mathbf{v}}(G^{\rm R-A})\hat{\sigma}_i(G^{\rm R-A})\}]. \tag{15}$$

Here $\hat{\mathbf{v}} = \partial_{\mathbf{k}}\mathcal{H}$ is the velocity operator in the direction of the applied electric field, $f(\epsilon)$ is the equilibrium Fermi distribution function, $G^{\rm R(A)}$ is the retarded (advanced) Green's function, and $G^{\rm R\pm A} = G^{\rm R} \pm G^{\rm A}$. Notice that Eq. (14) gives the intrinsic contribution, whereas Eq. (15) gives the extrinsic one. Based on their behavior under time reversal, we found that the spin-orbit field components that are *odd* in magnetization are of intrinsic origin, such as the damping-like torque $h_{\rm DL}^{\parallel,z}$, the 3m torque $h_{\rm 3m}^{\parallel}$, and the chiral torque $h_{\chi}^{\parallel,z}$, whereas the terms that are *even* in magnetization are extrinsic, such as the field-like torque $h_{\rm FL}^{\parallel,z}$ and the planar Hall torque $h_{\rm PH}^{\parallel,z}$.

To assess the relative magnitude of the different torque components and identify their physical origin, we compute the angular dependence of the fields when the magnetization rotates in the (**x**, **y**) plane, while the electric field is applied along x. Our results are reported in Fig. 3 for both intrinsic (a),(b) and extrinsic (c),(d) contributions in the cases of low (left panels) and high (right panels) band fillings. We analyze these results based on the angular dependence of the spin-orbit fields given by Eqs. (5) and (6), when there is linear and cubic spin-orbit coupling. In this scenario, we deduce that

$$\mathbf{h} = \begin{pmatrix} h_{\rm 3m}^{\parallel}\cos\phi - h_{\rm PH}^{\parallel}\sin 2\phi + h_{\rm DL}^{\parallel}\delta_{\rm DL}\cos 3\phi \\ -h_{\rm 3m}^{\parallel}\sin\phi + h_{\rm PH}^{\parallel}\cos 2\phi + h_{\rm FL}^{\parallel}(1+\delta_{\rm FL}\sin 3\phi) \\ h_{\rm DL}^{z}\cos\phi + h_{\rm PH}^{z}\sin 2\phi \end{pmatrix}. \tag{16}$$

From Fig. 3(a) it is clear that for h_x and h_y a threefold dependence related to $\delta_{\rm DL}$ and $\delta_{\rm FL}$ dominates at low band filling,

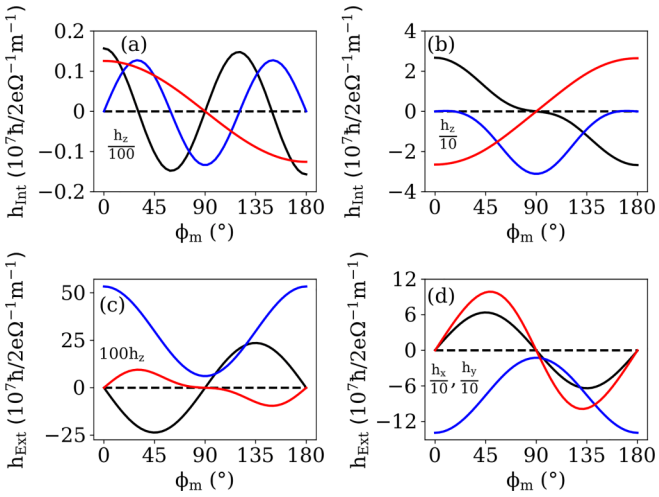

FIG. 3. Angular dependence of the effective field components h_x (black lines), h_y (blue lines), and h_z (red lines) when the magnetization rotates in the (x, y) plane. We indicate a scaling factor of a given component whenever necessary. The system's parameters are $t = 1$, $t_R = 0.1t$, $t_{R3} = 0.05t$, $\Delta = 0.5t$ and the homogeneous disorder $\Gamma = 0.1t$. The intrinsic (a), (b) and extrinsic (c), (d) contributions are plotted for $\mu = -5t$ (left panels) and $\mu = 2t$ (right panels). Our calculations reproduce our symmetry predictions in Eq. (16).

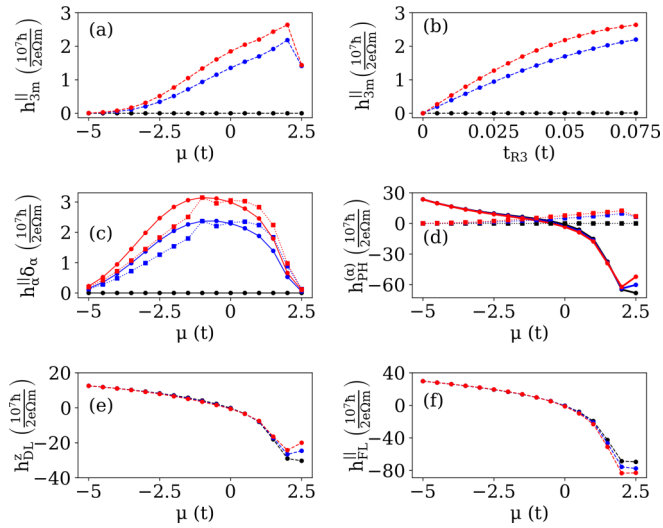

FIG. 4. Effective field's components extracted from fitting the numerical results with Eq. (16). The panels show (a) $h^{\parallel}_{3m}$, (c) $h^{\parallel}_{DL}\delta_{DL}$ (solid lines) and $h^{\parallel}_{FL}\delta_{FL}$ (dotted lines), (d) $h^{\parallel}_{PH}$ (solid lines) and h^{z}_{PH} (dotted lines), (e) h^{z}_{DL}, and (f) $h^{\parallel}_{FL}$ as a function of the chemical potential μ, for different values of the cubic spin-orbit coupling t_{R3} (black, blue, and red lines stand for $t_{R3} = 0,\ 0.05t,$ and $0.075t$). For completeness, panel (b) shows $h^{\parallel}_{3m}$ as a function of t_{R3} for different values of μ (black, blue, and red lines stand for $\mu = -5t,\ t,$ and $2t$).

while for h_z the term h^{z}_{DL} is predominant in this regime. Besides, $h^{\parallel}_{3m}$ can be identified through the h_y contribution at high band filling [Fig. 3(b)]. Regarding the extrinsic contributions, we notice from Fig. 3(c) that h_x and h_y are not trivial due to $h^{\parallel}_{PH}$ and $h^{\parallel}_{FL}$ at low band filling, whereas h^{z}_{PH} becomes relevant at high band filling in Fig. 3(d).

Analyzing the in-plane angular dependence of the field components, Fig. 3, with Eq. (16), one can extract the different torque contributions, reported on Fig. 4 as a function of t_{R3} and μ. From Figs. 4(a) and 4(b), $h^{\parallel}_{3m}$ requires cubic Rashba coupling and increases with the band filling, confirming its sensitivity to the trigonal warping of the Fermi surface. This behavior is different from $h^{\parallel}_{\alpha}\delta_{\alpha}$ (α = DL, FL), which is displayed in Fig. 4(c) and reaches a maximum close to $\mu = 0$ for $t_{R3} \neq 0$. The planar contributions $h^{\parallel}_{PH}$ and h^{z}_{PH} are depicted in Figs. 4(d) and they exhibit different behaviors with t_{R3} and μ: whereas h_{PH} does not require t_{R3} and follows a similar tendency to $h^{z}_{DL}$and $h^{\parallel}_{FL}$ [Figs. 4(e) and 4(f)], h^{z}_{PH} increases with the band filling and requires $t_{R3} \neq 0$. The salient features of the different torque components in C_{3v} systems are summarized in Table II.

TABLE II. Summary of the minimal model analysis.

Component	Physical origin	Source
$h^{\parallel}_{FL}$, h^{z}_{FL}, $h^{\parallel}_{PH}$	Extrinsic	Linear Rashba
h^{z}_{PH}, h^{z}_{3m}	Extrinsic	Linear + cubic Rashba
$h^{\parallel}_{DL}$, h^{z}_{DL}	Intrinsic	Linear Rashba
δ_{FL}, δ_{DL}	Intrinsic	Linear + cubic Rashba
$h^{\parallel}_{3m}$, $h^{\parallel}_{\chi}$, h^{z}_{χ}	Intrinsic	Linear + cubic Rashba

B. First principles case study: CuPt(111)/Co

We conclude this work by computing the spin-orbit torque in $L1_1$ CuPt(111)/Co from first principles. As explained above, this material has been recently experimentally demonstrated to host a sizable 3m torque [46]. We considered a CuPt/Co slab containing 12 layers, such that the $L1_1$ phase is made up of stacking elemental fcc layers along the [111] direction. We determine the band structure and spin textures by employing fully relativistic density functional theory. We describe the spin-orbit coupling within a fully relativistic pseudopotential formulation and used the generalized gradient approximation (GGA) for the exchange-correlation functional; the calculations are converged for a 400 Ry plane-wave cutoff for the real-space grid with a $13\times13\times1$ k-points sampling of the Brillouin zone. We used the conjugate gradient algorithm to minimize the atomic forces below 0.01 eV/Å. The momentum-resolved spin texture at the Fermi level is reported in Fig. 5 and displays a very clear hexagonal symmetry, suggesting an effectively large cubic spin-orbit coupling interaction.

The angular dependence of the intrinsic and extrinsic spin-orbit fields is reported on Figs. 6(a) and 6(b), respectively, when the magnetization is rotated in the (x, y) plane. The calculations are performed with broadening $\Gamma = 0.025$ eV in the zero temperature limit. The angular dependence is well reproduced by Eq. (16). The intrinsic spin-orbit torque is composed of the damping-like torque (h^z) and the 3m torque ($h^{x,y}$), with $h^{\parallel}_{3m}/h^{z}_{DL} \approx 0.67$, indicating that the 3m torque is about the same order of magnitude as the damping-like torque. The extrinsic torque is one order of magnitude larger and is composed of the field-like torque and the planar Hall torque. The possible differences between our numerical predictions

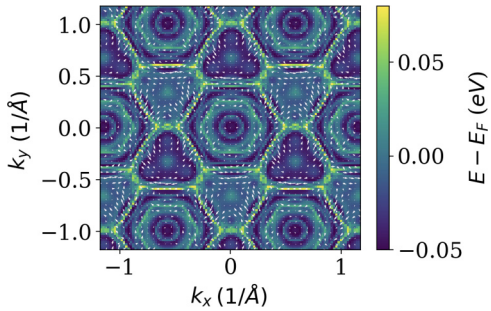

FIG. 5. Spin texture in momentum space close to Fermi level of a selected band of CuPt(111)/Co slab computed from first principles. A strong hexagonal symmetry is obtained suggesting the presence of a large cubic spin-orbit coupling interaction.

and our symmetry analysis in Eq. (16) can be explained by the neglect of higher-order terms in the character table expansion and the large values of cubic spin-orbit coupling. Nevertheless, we can extract $h^{\parallel}_{\mathrm{PH}}/h^{\parallel}_{\mathrm{FL}} \approx 1$ and $h^{z}_{\mathrm{PH}}/h^{\parallel}_{\mathrm{PH}} \approx 0.4$, meaning that the planar Hall torque is anisotropic and as large as the fieldlike torque, and shall therefore impact the magnetization switching and dynamics. We leave this question to further studies. We emphasize that the relative magnitude of the intrinsic to extrinsic torques is not meaningful since the extrinsic torque is inversely proportional to the disorder broadening Γ, which is taken as a (small) free parameter in our model.

C. Discussion and conclusion

The presence of these unconventional torques is particularly interesting for applications as they not only enable field-free switching but also impact the current-driven auto-oscillations. Our minimal model suggests that C_{3v} crystals could host such torques. Nonetheless, we emphasize that this is not a sufficient condition. As a matter of fact, in a previous study, we computed the spin-orbit torque in vanadium-based Janus transition metal dichalcogenides VSeTe and found no such torque, in spite of the similar crystal symmetries [52]. We attributed this absence to the fact that, in this material, the electronic transport is mostly driven by states at Γ point and therefore the crystal symmetries are not *imprinted* on the Bloch states. In contrast, in the $L1_1$ CuPt the Fermi surface shows a very strong warping, indicating that the Bloch states have a strong symmetry character and enabling the onset of the 3m torque as well as other unconventional torques. Since the indicator to the presence of this torque is the trigonal warping of the Fermi surface, many other materials could display such effects: for example, Bi-based topological insulators $(Bi,Sb)_2/(Se, Te)_3$ [62–64] and Bi_4Te_3 [65], but also possibly in the recently grown $LaAlO_3/EuTiO_3/SrTiO_3$ all-oxide heterostructure [66].

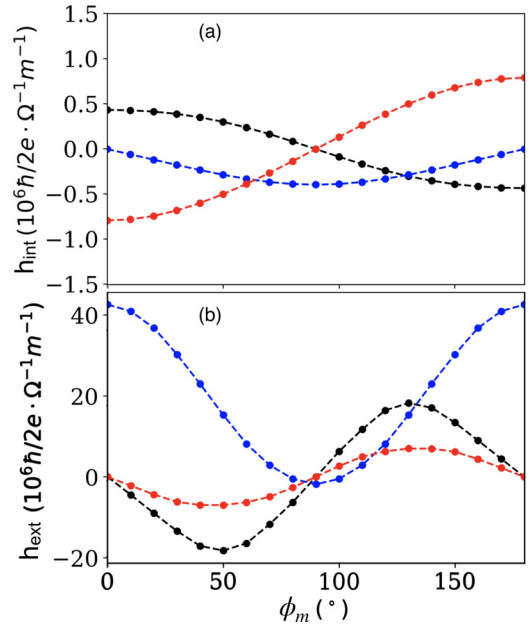

FIG. 6. Angular dependence of the intrinsic (top) and extrinsic (bottom) spin-orbit field components when the magnetization is rotated in the (x, y) plane. The black, blue, and red curves represent the x, y, and z components of the effective fields, respectively.

We conclude this work by emphasizing that other unconventional torques are yet to be found in low-symmetry crystals that could lead to original current-driven dynamics, as already reported in WTe_2/Py [29,31,32] and Fe_3GeTe_2 [49,50]. In this context, one needs to keep in mind that the general form of the spin-orbit field used in this work is obtained via a low-order expansion of the character table that is formally valid only when the spin-orbit coupling is smaller than the exchange. In materials where the spin-orbit coupling and the exchange are of the same order of magnitude, much more complex torques are expected.

ACKNOWLEDGMENTS

The authors thank L. Liu, J. Chen, K. Belashchenko, J. Medina, J. H. Garcia, and S. Roche for fruitful discussions. This work was supported by the ANR ORION project, Grant No. ANR-20-CE30-0022-01 of the French Agence Nationale de la Recherche. In addition, this research was partially financed by the ANR MNEMOSYN project, Grant No. ANR-21-GRF1-0005. D.G.O. and A.M. acknowledge support from the Excellence Initiative of Aix-Marseille Université–A*Midex, a French "Investissements d'Avenir" program.

[1] A. Manchon, J. Železný, I. M. Miron, T. Jungwirth, J. Sinova, A. Thiaville, K. Garello, and P. Gambardella, Current-induced spin-orbit torques in ferromagnetic and antiferromagnetic systems, Rev. Mod. Phys. **91**, 035004 (2019).

[2] I. M. Miron, G. Gaudin, S. Auffret, B. Rodmacq, A. Schuhl, S. Pizzini, J. Vogel, and P. Gambardella, Current-driven spin torque induced by the Rashba effect in a ferromagnetic metal layer, Nat. Mater. **9**, 230 (2010).

[3] L. Liu, T. Moriyama, D. C. Ralph, and R. A. Buhrman, Spin-Torque Ferromagnetic Resonance Induced by the Spin Hall Effect, Phys. Rev. Lett. **106**, 036601 (2011).

[4] Y.-W. Oh, S.-H. Chris Baek, Y. M. Kim, H. Y. Lee, K.-D. Lee, C.-G. Yang, E.-S. Park, K.-S. Lee, K.-W. Kim, G. Go, J.-R. Jeong, B.-C. Min, H.-W. Lee, K.-J. Lee, and B.-G. Park, Field-free switching of perpendicular magnetization through spin-orbit torque in antiferromagnet/ferromagnet/oxide structures, Nat. Nanotechnol. **11**, 878 (2016).

[5] S. Fukami, C. Zhang, S. Dutta Gupta, and H. Ohno, Magnetization switching by spin-orbit torque in an antiferromagnet/ferromagnet bilayer system, Nat. Mater. **15**, 535 (2016).

[6] Y.-C. Lau, D. Betto, K. Rode, J. M. D. Coey, and P. Stamenov, Spin-orbit torque switching without an external field using interlayer exchange coupling, Nat. Nanotechnol. **11**, 758 (2016).

[7] J. Wei, X. Wang, B. Cui, C. Guo, H. Xu, Y. Guang, Y. Wang, X. Luo, C. Wan, J. Feng, H. Wei, G. Yin, X. Han, and G. Yu, Field-free spinorbit torque switching in perpendicularly magnetized synthetic antiferromagnets, Adv. Funct. Mater. **32**, 2109455 (2022).

[8] S. H. C. Baek, V. P. Amin, Y. W. Oh, G. Go, S. J. Lee, G. H. Lee, K. J. Kim, M. D. Stiles, B. G. Park, and K. J. Lee, Spin currents and spin-orbit torques in ferromagnetic trilayers, Nat. Mater. **17**, 509 (2018).

[9] J. Ryu, R. Thompson, J. Y. Park, S. J. Kim, G. Choi, J. Kang, H. B. Jeong, M. Kohda, J. M. Yuk, J. Nitta, K. J. Lee, and B. G. Park, Efficient spinorbit torque in magnetic trilayers using all three polarizations of a spin current, Nat. Electron **5**, 217 (2022).

[10] V. P. Amin, J. Zemen, and M. D. Stiles, Interface-Generated Spin Currents, Phys. Rev. Lett. **121**, 136805 (2018).

[11] M. B. Lifshits and M. I. Dyakonov, Swapping Spin Currents: Interchanging Spin and Flow Directions, Phys. Rev. Lett. **103**, 186601 (2009).

[12] H. B. M. Saidaoui and A. Manchon, Spin-Swapping Transport and Torques in Ultrathin Magnetic Bilayers, Phys. Rev. Lett. **117**, 036601 (2016).

[13] Z. Luo, Q. Zhang, Y. Xu, Y. Yang, X. Zhang, and Y. Wu, Spin-Orbit Torque in a Single Ferromagnetic Layer Induced by Surface Spin Rotation, Phys. Rev. Appl. **11**, 064021 (2019).

[14] C. O. Pauyac, M. Chshiev, A. Manchon, and S. A. Nikolaev, Spin Hall and Spin Swapping Torques in Diffusive Ferromagnets, Phys. Rev. Lett. **120**, 176802 (2018).

[15] G. Yu, P. Upadhyaya, Y. Fan, J. G. Alzate, W. Jiang, K. L. Wong, S. Takei, S. A. Bender, L.-T. Chang, Y. Jiang, M. Lang, J. Tang, Y. Wang, Y. Tserkovnyak, P. K. Amiri, and K. L. Wang, Switching of perpendicular magnetization by spin-orbit torques in the absence of external magnetic fields, Nat. Nanotechnol. **9**, 548 (2014).

[16] A. Bose, D. D. Lam, S. Bhuktare, S. Dutta, H. Singh, Y. Jibiki, M. Goto, S. Miwa, and A. A. Tulapurkar, Observation of Anomalous Spin Torque Generated by a Ferromagnet, Phys. Rev. Appl. **9**, 064026 (2018).

[17] B. Cui, H. Wu, D. Li, S. A. Razavi, D. Wu, K. L. Wong, M. Chang, M. Gao, Y. Zuo, L. Xi, and K. L. Wang, Field-free spin-orbit torque switching of perpendicular magnetization by the rashba interface, ACS Appl. Mater. Interfaces **11**, 39369 (2019).

[18] A. Razavi, H. Wu, Q. Shao, C. Fang, B. Dai, K. Wong, X. Han, G. Yu, and K. L. Wang, Deterministic spin-orbit torque switching by a light-metal insertion, Nano Lett. **20**, 3703 (2020).

[19] M. G. Kang, J. G. Choi, J. Jeong, J. Y. Park, H. J. Park, T. Kim, T. Lee, K. J. Kim, K. W. Kim, J. H. Oh, D. D. Viet, J. R. Jeong, J. M. Yuk, J. Park, K. J. Lee, and B. G. Park, Electric-field control of field-free spin-orbit torque switching via laterally modulated Rashba effect in Pt/Co/AlO_x structures, Nat. Commun. **12**, 7111 (2021).

[20] C. K. Safeer, E. Jué, A. Lopez, L. Buda-Prejbeanu, S. Auffret, S. Pizzini, O. Boulle, I. M. Miron, and G. Gaudin, Spin-orbit torque magnetization switching controlled by geometry, Nat. Nanotechnol. **11**, 143 (2016).

[21] L. You, O. Lee, D. Bhowmik, D. Labanowski, J. Hong, J. Bokor, and S. Salahuddin, Switching of perpendicularly polarized nanomagnets with spin orbit torque without an external magnetic field by engineering a tilted anisotropy, Proc. Natl. Acad. Sci. USA **112**, 10310 (2015).

[22] L. Liu, Q. Qin, W. Lin, C. Li, Q. Xie, S. He, X. Shu, C. Zhou, Z. Lim, J. Yu, W. Lu, M. Li, X. Yan, S. J. Pennycook, and J. Chen, Current-induced magnetization switching in all-oxide heterostructures, Nat. Nanotechnol. **14**, 939 (2019).

[23] H. Li, G. Wang, D. Li, P. Hu, W. Zhou, S. Dang, X. Ma, T. Dai, S. Kang, F. Yu, X. Zhou, S. Wu, and S. Li, Field-free deterministic magnetization switching with ultralow current density in epitaxial Au/Fe 4 N bilayer films, ACS Appl. Mater. Interfaces **11**, 16965 (2019).

[24] X. Shu, L. Liu, J. Zhou, W. Lin, Q. Xie, T. Zhao, C. Zhou, S. Chen, H. Wang, J. Chai, Y. Ding, W. Chen, and J. Chen, Field-Free Switching of Perpendicular Magnetization Induced by Longitudinal Spin-Orbit-Torque Gradient, Phys. Rev. Appl. **17**, 024031 (2022).

[25] S. Chen, J. Yu, Q. Xie, X. Zhang, W. Lin, L. Liu, J. Zhou, X. Shu, R. Guo, Z. Zhang, and J. Chen, Free field electric switching of perpendicularly magnetized thin film by spin current gradient, ACS Appl. Mater. Interfaces **11**, 30446 (2019).

[26] A. Chernyshov, M. Overby, X. Liu, J. K. Furdyna, Y. Lyanda-Geller, and L. P. Rokhinson, Evidence for reversible control of magnetization in a ferromagnetic material by means of spinorbit magnetic field, Nat. Phys. **5**, 656 (2009).

[27] M. Endo, F. Matsukura, and H. Ohno, Current induced effective magnetic field and magnetization reversal in uniaxial anisotropy (Ga,Mn)As, Appl. Phys. Lett. **97**, 222501 (2010).

[28] C. Ciccarelli, L. Anderson, V. Tshitoyan, A. J. Ferguson, F. Gerhard, C. Gould, L. W. Molenkamp, J. Gayles, J. Zelezny, L. Smejkal, Z. Yuan, J. Sinova, F. Freimuth, and T. Jungwirth, Room-temperature spin-orbit torque in NiMnSb, Nat. Phys. **12**, 855 (2016).

[29] D. MacNeill, G. M. Stiehl, M. H. D. Guimaraes, R. A. Buhrman, J. Park, and D. C. Ralph, Control of spin-orbit torques through crystal symmetry in WTe_2/ferromagnet bilayers, Nat. Phys. **13**, 300 (2017).

[30] D. MacNeill, G. M. Stiehl, M. H. D. Guimarães, N. D. Reynolds, R. A. Buhrman, and D. C. Ralph, Thickness dependence of spin-orbit torques generated by WTe_2, Phys. Rev. B **96**, 054450 (2017).

[31] S. Shi, S. Liang, Z. Zhu, K. Cai, S. D. Pollard, Y. Wang, J. Wang, Q. Wang, P. He, J. Yu, G. Eda, G. Liang, and H. Yang, All-electric magnetization switching and Dzyaloshinskii–Moriya interaction in WTe_2/ferromagnet heterostructures, Nat. Nanotechnol. **14**, 945 (2019).

[32] Q. Xie, W. Lin, S. Sarkar, X. Shu, S. Chen, L. Liu, T. Zhao, C. Zhou, H. Wang, J. Zhou, S. Gradečak, and J. Chen, Field-free

magnetization switching induced by the unconventional spin-orbit torque from WTe2, APL Mater. **9**, 051114 (2021).

[33] I.-h. Kao, R. Muzzio, H. Zhang, M. Zhu, J. Gobbo, S. Yuan, D. Weber, R. Rao, J. Li, J. H. Edgar, J. E. Goldberger, J. Yan, D. G. Mandrus, J. Hwang, R. Cheng, J. Katoch, and S. Singh, Deterministic switching of a perpendicularly polarized magnet using unconventional spin orbit torques in WTe_2, Nat. Mater. **21**, 1029 (2022).

[34] F. Xue, C. Rohmann, J. Li, V. Amin, and P. Haney, Unconventional spin-orbit torque in transition metal dichalcogenide-ferromagnet bilayers from first-principles calculations, Phys. Rev. B **102**, 014401 (2020).

[35] M. H. Guimarães, G. M. Stiehl, D. MacNeill, N. D. Reynolds, and D. C. Ralph, Spin-Orbit Torques in NbSe2/Permalloy Bilayers, Nano Lett. **18**, 1311 (2018).

[36] J. Železný, Y. Zhang, C. Felser, and B. Yan, Spin-Polarized Current in Noncollinear Antiferromagnets, Phys. Rev. Lett. **119**, 187204 (2017).

[37] Y. Zhang, J. Zelezny, Y. Sun, J. V. D. Brink, and B. Yan, Spin Hall effect emerging from a noncollinear magnetic lattice without spin-orbit coupling, New J. Phys. **20**, 073028 (2018).

[38] M. Kimata, H. Chen, K. Kondou, S. Sugimoto, P. K. Muduli, M. Ikhlas, Y. Omori, T. Tomita, A. H. Macdonald, S. Nakatsuji, and Y. Otani, Magnetic and magnetic inverse spin Hall effects in a non-collinear antiferromagnet, Nature (London) **565**, 627 (2019).

[39] S. Ghosh, A. Manchon, and J. Železný, Unconventional Robust Spin-Transfer Torque in Noncollinear Antiferromagnetic Junctions, Phys. Rev. Lett. **128**, 097702 (2022).

[40] X. Chen, S. Shi, G. Shi, X. Fan, C. Song, X. Zhou, H. Bai, L. Liao, Y. Zhou, H. Zhang, A. Li, Y. Chen, X. Han, S. Jiang, Z. Zhu, H. Wu, X. Wang, D. Xue, H. Yang, and F. Pan, Observation of the antiferromagnetic spin Hall effect, Nat. Mater. **20**, 800 (2021).

[41] A. Bose, N. J. Schreiber, R. Jain, D. F. Shao, H. P. Nair, J. Sun, X. S. Zhang, D. A. Muller, E. Y. Tsymbal, D. G. Schlom, and D. C. Ralph, Tilted spin current generated by the collinear antiferromagnet ruthenium dioxide, Nat. Electron **5**, 267 (2022).

[42] H. Bai, L. Han, X. Y. Feng, Y. J. Zhou, R. X. Su, Q. Wang, L. Y. Liao, W. X. Zhu, X. Z. Chen, F. Pan, X. L. Fan, and C. Song, Observation of Spin Splitting Torque in a Collinear Antiferromagnet RuO_2, Phys. Rev. Lett. **128**, 197202 (2022).

[43] T. Nan, C. X. Quintela, J. Irwin, G. Gurung, D. F. Shao, J. Gibbons, N. Campbell, K. Song, S.-Y. Choi, L. Guo, R. D. Johnson, P. Manuel, R. V. Chopdekar, I. Hallsteinsen, T. Tybell, P. J. Ryan, J.-W. Kim, Y. Choi, P. G. Radaelli, D. C. Ralph *et al.*, Controlling spin current polarization through non-collinear antiferromagnetism, Nat. Commun. **11**, 4671 (2020).

[44] H. Bai, X. F. Zhou, H. W. Zhang, W. W. Kong, L. Y. Liao, X. Y. Feng, X. Z. Chen, Y. F. You, Y. J. Zhou, L. Han, W. X. Zhu, F. Pan, X. L. Fan, and C. Song, Control of spin-orbit torques through magnetic symmetry in differently oriented noncollinear antiferromagnetic Mn_3Pt, Phys. Rev. B **104**, 104401 (2021).

[45] K. Kondou, H. Chen, T. Tomita, M. Ikhlas, T. Higo, A. H. MacDonald, S. Nakatsuji, and Y. C. Otani, Giant field-like torque by the out-of-plane magnetic spin Hall effect in a topological antiferromagnet, Nat. Commun. **12**, 6491 (2021).

[46] S. Lee, C. Zhou, X. Shu, C. Li, T. Zhao, W. Lin, J. Deng, Q. Xie, S. Chen, J. Zhou, R. Guo, H. Wang, J. Yu, S. Shi, P. Yang, S. Pennycook, A. Manchon, and J. Chen, Symmetry-dependent field-free switching of perpendicular magnetization, Nat. Nanotechnol. **16**, 277 (2021).

[47] J. Železný, H. Gao, A. Manchon, F. Freimuth, Y. Mokrousov, J. Zemen, J. Mašek, J. Sinova, and T. Jungwirth, Spin-orbit torques in locally and globally non-centrosymmetric crystals: Antiferromagnets and ferromagnets, Phys. Rev. B **95**, 014403 (2017).

[48] C. Gong and X. Zhang, Two-dimensional magnetic crystals and emergent heterostructure devices, Science **363**, eaav4450 (2019).

[49] Ø. Johansen, V. Risinggård, A. Sudbø, J. Linder, and A. Brataas, Current Control of Magnetism in Two-Dimensional Fe_3GeTe_2, Phys. Rev. Lett. **122**, 217203 (2019).

[50] K. Zhang, S. Han, Y. Lee, M. J. Coak, J. Kim, I. Hwang, S. Son, J. Shin, M. Lim, D. Jo, K. Kim, D. Kim, H. W. Lee, and J. G. Park, Gigantic Current Control of Coercive Field and Magnetic Memory Based on Nanometer-Thin Ferromagnetic van der Waals Fe_3GeTe_2, Adv. Mater. **33**, 2004110 (2021).

[51] S. Laref, K.-w. Kim, and A. Manchon, Elusive Dzyaloshinskii-Moriya interaction in monolayer Fe_3GeTe_2, Phys. Rev. B **102**, 060402(R) (2020).

[52] I. Smaili, S. Laref, J. H. Garcia, U. Schwingenschlögl, S. Roche, and A. Manchon, Janus monolayers of magnetic transition metal dichalcogenides as an all-in-one platform for spin-orbit torque, Phys. Rev. B **104**, 104415 (2021).

[53] M. S. Dresselhaus, *Group Theory: Application to the Physics of Condensed Matter* (Springer, New York, 2008).

[54] M. J. Lax, *Symmetry Principles in Solid State and Molecular Physics* (Dover Publications, Dover, UK, 2012).

[55] L. Liu, C.-F. Pai, D. C. Ralph, and R. A. Buhrman, Magnetic Oscillations Driven by the Spin Hall Effect in 3-Terminal Magnetic Tunnel Junction Devices, Phys. Rev. Lett. **109**, 186602 (2012).

[56] V. E. Demidov, S. Urazhdin, H. Ulrichs, V. Tiberkevich, A. Slavin, D. Baither, G. Schmitz, and S. O. Demokritov, Magnetic nano-oscillator driven by pure spin current, Nat. Mater. **11**, 1028 (2012).

[57] D. Kurebayashi and N. Nagaosa, Theory of current-driven dynamics of spin textures on the surface of a topological insulator, Phys. Rev. B **100**, 134407 (2019).

[58] Y. Imai, T. Yamaguchi, A. Yamakage, and H. Kohno, Spintronic properties of topological surface Dirac electrons with hexagonal warping, Phys. Rev. B **103**, 054402 (2021).

[59] Y.-L. Zhou, H.-J. Duan, Y.-J. Wu, M.-X. Deng, L. Wang, D. Culcer, and R.-Q. Wang, Nonlinear antidamping spin-orbit torque originating from intraband transport on the warped surface of a topological insulator, Phys. Rev. B **105**, 075415 (2022).

[60] J. Y. Li, R. Q. Wang, M. X. Deng, and M. Yang, In-plane magnetization effect on current-induced spin-orbit torque in a ferromagnet/topological insulator bilayer with hexagonal warping, Phys. Rev. B **99**, 155139 (2019).

[61] V. Bonbien and A. Manchon, Symmetrized decomposition of the Kubo-Bastin formula, Phys. Rev. B **102**, 085113 (2020).

[62] Y. L. Chen, J. G. Analytis, J.-H. Chu, Z. K. Liu, S.-K. Mo, X. L. Qi, H. J. Zhang, D. H. Lu, X. Dai, Z. Fang, S. C. Zhang, I. R. Fisher, Z. Hussain, and Z.-X. Shen, Experimental realization of a three-dimensional topological insulator, Bi_2Te_3, Science **325**, 178 (2009).

[63] D. Hsieh, Y. Xia, D. Qian, L. Wray, J. H. Dil, F. Meier, J. Osterwalder, L. Patthey, J. G. Checkelsky, N. P. Ong, A. V. Fedorov, H. Lin, A. Bansil, D. Grauer, Y. S. Hor, R. J. Cava, and M. Z. Hasan, A tunable topological insulator in the spin helical Dirac transport regime, Nature (London) **460**, 1101 (2009).

[64] Z. Alpichshev, J. G. Analytis, J. H. Chu, I. R. Fisher, Y. L. Chen, Z. X. Shen, A. Fang, and A. Kapitulnik, STM Imaging of Electronic Waves on the Surface of Bi_2Te_3: Topologically Protected Surface States and Hexagonal Warping Effects, Phys. Rev. Lett. **104**, 016401 (2010).

[65] T. Chagas, O. A. Ashour, G. A. S. Ribeiro, W. S. Silva, Z. Li, S. G. Louie, R. Magalhães-Paniago, and Y. Petroff, Multiple strong topological gaps and hexagonal warping in Bi_4Te_3, Phys. Rev. B **105**, L081409 (2022).

[66] Y. Chen, M. D'Antuono, N. B. Brookes, G. M. De Luca, R. Di Capua, E. Di Gennaro, G. Ghiringhelli, C. Piamonteze, D. Preziosi, B. Jouault, M. Cabero, J. M. González-Calbet, C. León, J. Santamaria, A. Sambri, D. Stornaiuolo, and M. Salluzzo, Ferromagnetic quasi-two-dimensional electron gas with trigonal crystal field splitting, ACS Appl. Electron. Mater. **4**, 3226 (2022).